

The CMB temperature bispectrum induced by cosmic strings

Mark Hindmarsh*

Department of Physics & Astronomy, University of Sussex, Brighton, BN19QH, United Kingdom

Christophe Ringeval[†] and Teruaki Suyama[‡]

*Theoretical and Mathematical Physics Group, Centre for Particle Physics and Phenomenology,
Lowain University, 2 Chemin du Cyclotron, 1348 Lowain-la-Neuve, Belgium*

(Dated: May 30, 2019)

The Cosmic Microwave Background bispectrum of the temperature anisotropies induced by a network of cosmic strings is derived for small angular scales, under the assumption that the principal cause of temperature fluctuations is the Gott–Kaiser–Stebbins (GKS) effect. We provide analytical expressions for equilateral and all isosceles triangle configurations in Fourier space. Such configurations generically lead to a negative bispectrum with a power law decay ℓ^{-6} for multipole ℓ . At $\ell \sim 500$ the cosmic string GKS effect contributes approximately the same equilateral signal as an inflationary model with $|f_{\text{NL}}| \simeq 10^3$, if the strings contribute about 10% of the temperature power spectrum at $\ell = 10$. However, collapsed triangles are found to be associated with a positive bispectrum whereas the squeezed triangles still exhibit negative values. The overall amplitude of all isosceles configurations is amplified as the inverse cube of the angle and diverges for flat triangles. We then compare our analytical estimates to a direct computation of the bispectrum from a set of 300 statistically independent temperature maps obtained from Nambu–Goto cosmic string simulations in a Friedmann–Lemaître–Robertson–Walker (FLRW) universe. We find good agreement for the overall amplitude, the power law behaviour and angle dependency of the various triangle configurations.

PACS numbers: 98.80.Cq, 98.70.Vc

I. INTRODUCTION

Cosmic strings are line-like objects formed in the early universe [1, 2, 3]. They could be solitons in field theories with spontaneously broken symmetries [4], singular solutions with cylindrical symmetry in supergravity theories [5] or fundamental objects in string theory [6]. They may form in thermal phase transitions [4], at the end of hybrid inflation [7, 8, 9], or by tachyon condensation at the end of brane inflation when brane and anti-brane annihilate [10, 11]. If cosmic strings are added to the standard power-law Λ CDM model, the Cosmic Microwave Background (CMB) data is fitted even better [12, 13] if the fraction of the temperature power spectrum (at $\ell = 10$) due to strings f_{10} is about 0.1. There is therefore strong motivation to develop further tests for strings in future CMB data, which provide the cleanest and best understood cosmological string signals [14]. Calculations of the polarisation B-mode [15, 16] show that a promising line of attack for the near future is to look for a signal peaked between $\ell = 600$ to 1000. Simulations of Planck data show that it will be sensitive down to $f_{10} \simeq 0.01$, and that there is no danger of confusing strings with inflationary tensor perturbations [15]. Perhaps the most characteristic signal in the CMB comes from the Gott–Kaiser–Stebbins (GKS) effect [17, 18], which is due to

the gravitational lensing of photons passing near a moving string. This produces a discontinuity in the apparent temperature approximately proportional to the transverse velocity of the string v and the string tension U :

$$\delta T \sim 8\pi(GU)vT_{\text{CMB}}, \quad (1)$$

where G is Newton’s constant. Given that strings move with a mean square (RMS) velocity of between 0.25 and 0.36 [19, 20] we would expect to see discontinuities δT of up to about $1 \mu\text{K}$. Recent calculations of the integrated Sachs–Wolf CMB signal at small angular scales have shown that the angular power spectrum it produces decreases slowly, approximately $\ell^{-0.9}$ at high multipole moment ℓ [21]. If $f_{10} \simeq 0.1$ strings should dominate the adiabatic temperature power spectrum for $\ell \gtrsim 3000$, and remain above the thermal Sunyaev–Zel’dovich effect. This fraction corresponds to $GU \simeq 0.7 \times 10^{-6}$ for strings in the Abelian Higgs model [13]. The slow power-law decrease in the power spectrum is quite close to a prediction of the small scale power spectrum using the string correlation functions in a Gaussian approximation [22], which gave a temperature anisotropy power going as ℓ^{-1} . The non-Gaussian nature of the maps exhibited in [21], as for example exhibited by the skewness of the distribution of the 1-point function, immediately motivates an attempt to generalise the calculation to higher-order correlators, and in particular the 3-point function or bispectrum, which will become increasingly well characterised by future CMB data [23, 24]. This paper reports on the results of this calculation. It is found that the bispectrum (for an equilateral arrangement of wavevectors \mathbf{k} of the Fourier transformed temperature map) is negative

*Electronic address: m.b.hindmarsh@sussex.ac.uk

[†]Electronic address: christophe.ringeval@uclouvain.be

[‡]Electronic address: teruaki.suyama@uclouvain.be

and decreases as $|\mathbf{k}|^{-6}$. It is proportional to $(GU)^3$ and hence to the power spectrum raised to the 3/2 power. The scale of the non-linearity parameter f_{NL} , defined by dividing the bispectrum by the square of the power spectrum, is therefore potentially large, going as $(GU)^{-1}$.

II. ANALYTICAL BISPECTRUM

A. Gott-Kaiser-Stebbins effect

We work in the flat sky approximation, and define transverse coordinates \mathbf{x} measured in radians. The wave number \mathbf{k} is related to the multipole moment ℓ by [25, 26]

$$k^2 \simeq \ell(\ell + 1). \quad (2)$$

The anisotropy power $\ell(\ell + 1)C_\ell$ is then approximately equal to $k^2|\delta T_{\mathbf{k}}|^2$, where $\delta T_{\mathbf{k}}$ is the Fourier transform of the temperature fluctuation,

$$\delta T_{\mathbf{k}} = \int d\mathbf{x} \delta T e^{i\mathbf{k}\cdot\mathbf{x}}. \quad (3)$$

We will also define $\Theta(\mathbf{x}) = \delta T(\mathbf{x})/T_{\text{CMB}}$. String space-time coordinates will be denoted $X^\mu(\tau, \sigma)$, where τ and σ are timelike and spacelike worldsheet coordinates respectively. In the temporal gauge the $X^0 = \tau$ (where the worldsheet time is identified with the background time coordinate) the (corrected) GKS formula is [22]

$$\nabla^2 \Theta = -8\pi GU \int d\sigma \left[\dot{\mathbf{X}} - \frac{(\dot{\mathbf{X}} \cdot \hat{p})}{(\dot{\mathbf{X}} \cdot \hat{p})} \dot{\mathbf{X}} \right] \cdot \nabla \delta^{(2)}(\mathbf{x} - \mathbf{X}), \quad (4)$$

where $\hat{p}^\mu = p^\mu/E$, and worldsheet variables are evaluated at the retarded time $t_r = t + z - X^3(\sigma, t_r)$, when the CMB photons (taken to be moving in the $-z$ direction) pass the string. The expression is greatly simplified in the light cone gauge,

$$X^+(\sigma, \tau) = \tau, \quad (5)$$

where $X^\pm = X^0 \pm X^3$. The time parameter τ then labels the intersections with a set of null hyperplanes with the worldsheet: the photon geodesics $Z^\mu = x^\mu + \lambda p^\mu$ form just such a set. Then we find

$$\nabla^2 \Theta = -8\pi GU \int d\sigma \dot{\mathbf{X}} \cdot \nabla \delta^{(2)}(\mathbf{x} - \mathbf{X}), \quad (6)$$

where worldsheet quantities are now evaluated at $\tau = x^+ = t + z$. In Fourier space the equation becomes

$$-k^2 \Theta_{\mathbf{k}} = i\epsilon k_A \int d\sigma \dot{X}^A(\sigma) e^{i\mathbf{k}\cdot\mathbf{X}(\sigma)}, \quad (7)$$

where we have defined

$$\epsilon = 8\pi GU, \quad (8)$$

and $A = 1, 2$ with implicit summation on repeated indices. It is now clear that the power spectrum, bispectrum, and higher order correlators can be evaluated in terms of correlation functions of the string network, as projected onto our backward light cone. In the next section we will introduce the relevant correlation functions and discuss their important features.

B. String correlation functions

We denote the transverse coordinates of the string, $X^A(\sigma)$. The basic two point functions are

$$\langle \dot{X}^A(\sigma) \dot{X}^B(\sigma') \rangle, \quad \langle \dot{X}^A(\sigma) \dot{X}^B(\sigma') \rangle, \quad \langle \dot{X}^A(\sigma) \dot{X}^B(\sigma') \rangle, \quad (9)$$

where the angle brackets denote an average over an ensemble of strings. The starting assumption is that the string ensemble is well-approximated by a Gaussian process: that is, all correlators can be calculated in terms of the two point functions. We now make some assumptions about the ensemble: (i) rotation, reflection and translation invariance of the transverse coordinates; and (ii) worldsheet reflection and translation invariance. Then there are three independent correlation functions:

$$\langle \dot{X}^A(\sigma) \dot{X}^B(\sigma') \rangle = \frac{1}{2} \delta^{AB} V(\sigma - \sigma'), \quad (10)$$

$$\langle \dot{X}^A(\sigma) \dot{X}^B(\sigma') \rangle = \frac{1}{2} \delta^{AB} T(\sigma - \sigma'), \quad (11)$$

$$\langle \dot{X}^A(\sigma) \dot{X}^B(\sigma') \rangle = \frac{1}{2} \delta^{AB} M_1(\sigma - \sigma'). \quad (12)$$

A fourth,

$$M_2(\sigma) = \langle \dot{X}^A(\sigma) \dot{X}^B(0) \rangle \epsilon^{AB}, \quad (13)$$

vanishes because of the symmetry $X^1 \leftrightarrow X^2$ (this point was overlooked in Ref. [22]). The functions V and T are symmetric in their argument, while M_1 is antisymmetric. The forms of the correlators are sketched in Fig. 1 (see also [20]). For later convenience two other correlators will be defined:

$$\Gamma(\sigma - \sigma') \equiv \left\langle [\mathbf{X}(\sigma) - \mathbf{X}(\sigma')]^2 \right\rangle \quad (14)$$

$$= \int_{\sigma'}^{\sigma} d\sigma_1 \int_{\sigma'}^{\sigma} d\sigma_2 T(\sigma_1 - \sigma_2), \quad (15)$$

$$\Pi(\sigma - \sigma') \equiv \left\langle [\mathbf{X}(\sigma) - \mathbf{X}(\sigma')] \cdot \dot{\mathbf{X}}(\sigma') \right\rangle \quad (16)$$

$$= \int_{\sigma'}^{\sigma} d\sigma_1 M_1(\sigma_1 - \sigma'), \quad (17)$$

There are integral constraints arising from the fact that the average velocity of the strings vanishes on large scale:

$$\int d\sigma V(\sigma) \rightarrow 0, \quad \int d\sigma M_1(\sigma) \rightarrow 0. \quad (18)$$

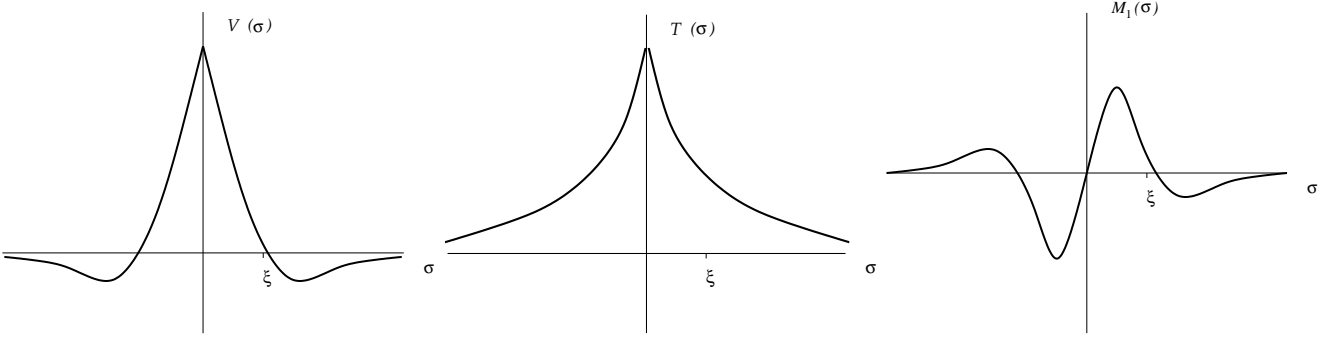


FIG. 1: Sketches of string correlation functions $V(\sigma)$ (velocity-velocity), $T(\sigma)$ (tangent-tangent) and $M_1(\sigma)$ (velocity-tangent), as a function of the string worldsheet spacelike separation σ , defined in Eqs. (10) to (12)

The important asymptotic forms are:

$$V(\sigma) \rightarrow \begin{cases} \bar{v}^2 & \sigma \rightarrow 0 \\ 0 & \sigma \rightarrow \infty \end{cases}, \quad (19)$$

$$\Gamma(\sigma) \rightarrow \begin{cases} \bar{t}^2 \sigma^2 & \sigma \rightarrow 0 \\ \hat{\xi} \sigma & \sigma \rightarrow \infty \end{cases}, \quad (20)$$

$$\Pi(\sigma) \rightarrow \begin{cases} \frac{1}{2} \frac{c_0}{\xi} \sigma^2 & \sigma \rightarrow 0 \\ 0 & \sigma \rightarrow \infty \end{cases}, \quad (21)$$

where we have defined four parameters

$$\hat{\xi} = \Gamma'(\infty), \quad (22)$$

$$\bar{v}^2 = \langle \dot{\mathbf{X}}^2 \rangle, \quad (23)$$

$$\bar{t}^2 = \langle \dot{\mathbf{X}}^2 \rangle, \quad (24)$$

$$c_0 = \hat{\xi} \langle \ddot{\mathbf{X}} \cdot \dot{\mathbf{X}} \rangle. \quad (25)$$

The correlation length $\hat{\xi}$ is the projected correlation length on the backward lightcone, \bar{t}^2 is the mean square projected tangent vector (of order unity), \bar{v}^2 is the mean square projected velocity (again of order unity), and c_0 is the correlation between the projected velocity and curvature.

C. Light cone gauge equations

In Minkowski space, the Nambu–Goto action leads to the equations of motion and constraints

$$\ddot{X}^\mu - \ddot{X}^\mu = 0, \quad \dot{X}^2 + \dot{X}^2 = 0, \quad \dot{X} \cdot \dot{X} = 0. \quad (26)$$

The light-cone gauge consists of choosing $\tau = X^+ = X^0 + X^3$. Hence

$$\dot{X}^- = \dot{X}_A \dot{X}^A + \dot{X}_A \dot{X}^A, \quad \dot{X}^- = 2\dot{X}_A \dot{X}^A. \quad (27)$$

The equations of motion in a FLRW background follow from the Nambu–Goto action

$$\begin{aligned} S &= -U \int d\tau d\sigma \sqrt{-\gamma} \\ &= -U \int d\tau d\sigma a^2(X^0) \sqrt{-\dot{X}^2 \dot{X}^2 + (\dot{X} \cdot \dot{X})^2}, \end{aligned} \quad (28)$$

where γ is the determinant of the induced metric along the string worldsheet, and $a(X^0)$ is the scale factor. With the standard gauge choice $\dot{X} \cdot \dot{X} = 0$, we find

$$\begin{aligned} \ddot{X}^\mu + \left(\frac{\dot{\epsilon}}{\epsilon} + 2\frac{\dot{a}}{a} \right) \dot{X}^\mu - \frac{1}{\epsilon} \frac{\partial}{\partial \sigma} \left(\frac{1}{\epsilon} \frac{\partial X^\mu}{\partial \sigma} \right) \\ - 2\frac{1}{a} \frac{da}{dX^0} \frac{1}{\epsilon} \frac{\partial X^0}{\partial \sigma} \frac{1}{\epsilon} \frac{\partial X^\mu}{\partial \sigma} + 2\delta_0^\mu \frac{1}{a} \frac{da}{dX^0} \dot{X}^2 = 0, \end{aligned} \quad (29)$$

where $\epsilon = \sqrt{-\dot{X}^2/\dot{X}^2}$. The light-cone gauge choice $X^+ = \tau$ produces as the equation of motion for X^+

$$\frac{\dot{\epsilon}}{\epsilon} + 2\mathcal{H}(\dot{X}^0 + \dot{X}^2) = 0, \quad (30)$$

where $\mathcal{H} = d \ln a / dX^0$ is the conformal Hubble parameter. The equation for the transverse components is

$$\begin{aligned} \ddot{\mathbf{X}} + 2\mathcal{H} \frac{1}{\epsilon^2} (\dot{\mathbf{X}}^2) \dot{\mathbf{X}} - \frac{1}{\epsilon} \frac{\partial}{\partial \sigma} \left(\frac{1}{\epsilon} \frac{\partial \mathbf{X}}{\partial \sigma} \right) \\ - 2\mathcal{H} \frac{1}{\epsilon^2} (\dot{\mathbf{X}} \cdot \dot{\mathbf{X}}) \dot{\mathbf{X}} = 0. \end{aligned} \quad (31)$$

In a FLRW background, assuming that $\langle \dot{\mathbf{X}}^2 \rangle$ is constant, and neglecting higher-order correlations between \mathcal{H} , $\dot{\mathbf{X}}$ and $\dot{\mathbf{X}}$, we find

$$\begin{aligned} \left\langle \frac{\partial^2 \mathbf{X}}{\partial s^2} \cdot \dot{\mathbf{X}} \right\rangle &= 2\bar{\mathcal{H}} \left\langle \left(\frac{\partial \mathbf{X}}{\partial s} \right)^2 \dot{\mathbf{X}}^2 \right\rangle \\ &\quad - 2\bar{\mathcal{H}} \left\langle \left(\dot{\mathbf{X}} \cdot \frac{\partial \mathbf{X}}{\partial s} \right)^2 \right\rangle, \end{aligned} \quad (32)$$

where we have defined $ds = \varepsilon d\sigma$, and where $\bar{\mathcal{H}}$ is the conformal Hubble parameter averaged over the string ensemble at fixed $\tau = X^+$, which will select the value where there is most string, i.e. at decoupling.

If one we assume that the string ensemble is approximately Gaussian in $\dot{\mathbf{X}}$ and $\dot{\mathbf{X}}/\varepsilon$, it is not hard to show that the right hand side reduces to

$$\left\langle \frac{\partial^2 \mathbf{X}}{\partial s^2} \cdot \dot{\mathbf{X}} \right\rangle = \bar{\mathcal{H}} \left(\left\langle \dot{\mathbf{X}}^2 \right\rangle \left\langle \dot{\mathbf{X}}^2 \right\rangle - \left\langle \dot{\mathbf{X}} \cdot \dot{\mathbf{X}} \right\rangle^2 \right). \quad (33)$$

The last term vanishes, so the cross correlator simplifies to $\bar{\mathcal{H}}\bar{v}^2\bar{t}^2$ which is positive. From Eq. (25), one gets that in a FLRW background, a string network should exhibit $c_0 > 0$. We see also that it vanishes in Minkowski space, which can be viewed as a consequence of time reversal invariance. As shown in the next sections, the temperature bispectrum vanishes when the correlator Π does, and so the generation of a bispectrum by strings simply requires the breaking of time reversal invariance, as it is in a FLRW background¹.

D. Temperature power spectrum at small angular scales

The power spectrum at small angular scales, where the GKS effect [17, 27] is held to be dominant, was calculated in Ref. [22], and the calculation is recapped here for completeness. The Fourier transform of the temperature fluctuation given in Eq. (6) reads

$$\Theta_{\mathbf{k}} = \int d^2x \frac{\delta T}{T} e^{i\mathbf{k}\cdot\mathbf{x}}, \quad (34)$$

and hence is given by Eq. (7). The power spectrum is defined by

$$\langle \Theta_{\mathbf{k}_1} \Theta_{\mathbf{k}_2} \rangle = P(k_1) (2\pi)^2 \delta(\mathbf{k}_1 + \mathbf{k}_2). \quad (35)$$

With our conventions we need a box of formal area $\mathcal{A} = (2\pi)^2 \delta(0)$ to express the power spectrum

$$P(k) = \varepsilon^2 \frac{k_A k_B}{A k^4} \int d\sigma d\sigma' \left\langle \dot{X}^A(\sigma) \dot{X}^B(\sigma') \times e^{i\mathbf{k}\cdot[\mathbf{X}(\sigma) - \mathbf{X}(\sigma')]} \right\rangle. \quad (36)$$

With our assumptions about the string correlation functions, the ensemble average can be reduced to

$$P(k) = \frac{1}{2} \varepsilon^2 \frac{1}{A k^2} \int d\sigma d\sigma' \left[V(\sigma - \sigma') + \frac{1}{2} k^2 \Pi^2(\sigma - \sigma') \right] e^{-k^2 \Gamma(\sigma - \sigma')/4}. \quad (37)$$

We now derive the asymptotic behaviour of $P(k)$ as $(k\xi)$ gets large. The contribution to the power spectrum from the mixed correlator M_1 can be shown to be subdominant at high k [22], and so we need examine only the first term in the power spectrum of Eq. (37),

$$P(k) = \varepsilon^2 \frac{1}{4A k^2} \int d\sigma_+ d\sigma_- V(\sigma_-) e^{-k^2 \Gamma(\sigma_-)/4}, \quad (38)$$

where $\sigma_{\pm} = \sigma \pm \sigma'$. For $k\hat{\xi} \gg 1$, we find

$$k^2 P(k) \simeq \varepsilon^2 \sqrt{\pi} \frac{L \hat{\xi} \bar{v}^2}{\mathcal{A} \bar{t}} \frac{1}{(k\hat{\xi})}, \quad (39)$$

where L is the total transverse light-cone gauge length of string in the box of area \mathcal{A} . The power spectrum given in Ref. [28] was consistent with k^{-1} , and the amplitude was surprisingly close for such a crude estimate. Fraisse et al. [21] have a slightly different small-scale angular power spectrum: $k^2 P(k) \sim k^{-p}$ with $p \simeq -0.89$. This can be explained if $\Gamma(\sigma) \sim \sigma^{2/p}$ on the relevant scales. This correlation function controls how far on average one moves in the transverse coordinates as one moves along the string: $p = 1$ would correspond to straight lines, while $p = 2$ to a Brownian random walk. A power less than one is suggestive of a cloud of zero-dimensional objects along the string worldsheet which may be the signature of small loop production.

E. Temperature bispectrum from strings at small angular scales

In the flat sky approximation the three point temperature correlation function or bispectrum is defined as

$$\langle \Theta_{\mathbf{k}_1} \Theta_{\mathbf{k}_2} \Theta_{\mathbf{k}_3} \rangle = B(\mathbf{k}_1, \mathbf{k}_2, \mathbf{k}_3) (2\pi)^2 \delta(\mathbf{k}_1 + \mathbf{k}_2 + \mathbf{k}_3). \quad (40)$$

We again need to normalise by a formal area factor $\mathcal{A} = (2\pi)^2 \delta(0)$ to obtain an expression in terms of a string expectation value

$$B(\mathbf{k}_1, \mathbf{k}_2, \mathbf{k}_3) = i \varepsilon^3 \frac{1}{\mathcal{A}} \delta_{A\bar{A}} \delta_{B\bar{B}} \delta_{C\bar{C}} \frac{k_1^{\bar{A}} k_2^{\bar{B}} k_3^{\bar{C}}}{k_1^{\bar{A}} k_2^{\bar{B}} k_3^{\bar{C}}} \times \int d\sigma_1 d\sigma_2 d\sigma_3 \left\langle \dot{X}_1^{\bar{A}} \dot{X}_2^{\bar{B}} \dot{X}_3^{\bar{C}} e^{i\delta^{ab} \mathbf{k}_a \cdot \mathbf{X}_b} \right\rangle, \quad (41)$$

with $\dot{X}_a^{\bar{A}} = \dot{X}^{\bar{A}}(\sigma_a)$, $a, b \in \{1, 2, 3\}$, and $\mathbf{k}_1 + \mathbf{k}_2 + \mathbf{k}_3 = 0$. With the Gaussian assumption, the ensemble average of the string observables is lengthy but straightforward. Defining

$$C^{ABC} \equiv \dot{X}_1^{\bar{A}} \dot{X}_2^{\bar{B}} \dot{X}_3^{\bar{C}}, \quad D \equiv \delta^{ab} \mathbf{k}_a \cdot \mathbf{X}_b, \quad (42)$$

we have

$$\langle C^{ABC} e^{iD} \rangle = i \langle C^{ABC} D \rangle e^{-\frac{1}{2} \langle D^2 \rangle}, \quad (43)$$

¹ We thank B. Wandelt for explaining this point to us.

and hence

$$B(\mathbf{k}_1, \mathbf{k}_2, \mathbf{k}_3) = -\epsilon^3 \frac{1}{\mathcal{A}} \frac{k_{1A} k_{2B} k_{3C}}{k_1^2 k_2^2 k_3^2} \times \int d\sigma_1 d\sigma_2 d\sigma_3 \langle C^{ABCD} \rangle e^{-\frac{1}{2} \langle D^2 \rangle}. \quad (44)$$

We first evaluate the correlator

$$\begin{aligned} \langle C^{ABCD} \rangle &= \langle \dot{X}_1^A \dot{X}_2^B \dot{X}_3^C \mathbf{k}^a \cdot \mathbf{X}_a \rangle \\ &= \langle \dot{X}_1^A \dot{X}_2^B \rangle \langle \dot{X}_3^C \mathbf{k}^a \cdot \mathbf{X}_a \rangle + \langle \dot{X}_3^C \dot{X}_1^A \rangle \langle \dot{X}_2^B \mathbf{k}^a \cdot \mathbf{X}_a \rangle \\ &+ \langle \dot{X}_2^B \dot{X}_3^C \rangle \langle \dot{X}_1^A \mathbf{k}^a \cdot \mathbf{X}_a \rangle. \end{aligned} \quad (45)$$

The velocity correlators have already been given in Eq. (10). The mixed correlators are most easily evaluated using variations on the theme

$$\begin{aligned} \mathbf{k}^a \cdot \mathbf{X}_a &= \mathbf{k}_1 \cdot (\mathbf{X}_1 - \mathbf{X}_3) + \mathbf{k}_2 \cdot (\mathbf{X}_2 - \mathbf{X}_3) \\ &= \mathbf{k}_1 \cdot \mathbf{X}_{13} + \mathbf{k}_2 \cdot \mathbf{X}_{23}, \end{aligned} \quad (46)$$

where $\mathbf{X}_{ab} \equiv \mathbf{X}_a - \mathbf{X}_b$. For example,

$$\langle \dot{X}_1^A \mathbf{k}^a \cdot \mathbf{X}_a \rangle = k_2^D \langle \dot{X}_1^A X_{21}^D \rangle + k_3^D \langle \dot{X}_1^A X_{31}^D \rangle. \quad (47)$$

Using the definition of the correlator $\Pi(\sigma)$ in Eq. (17),

$$\langle \dot{X}_1^A \mathbf{k}^a \cdot \mathbf{X}_a \rangle = \frac{1}{2} k_2^A \Pi(\sigma_{21}) + \frac{1}{2} k_3^A \Pi(\sigma_{31}), \quad (48)$$

where $\sigma_{ab} = \sigma_a - \sigma_b$. Substituting for the velocity correlators

$$\begin{aligned} \langle C^{ABCD} \rangle &= \frac{1}{4} \delta^{AB} [k_1^C \Pi(\sigma_{13}) + k_2^C \Pi(\sigma_{23})] V(\sigma_{12}) \\ &+ \frac{1}{4} \delta^{CA} [k_1^B \Pi(\sigma_{12}) + k_3^B \Pi(\sigma_{32})] V(\sigma_{31}) \\ &+ \frac{1}{4} \delta^{BC} [k_2^A \Pi(\sigma_{21}) + k_3^A \Pi(\sigma_{31})] V(\sigma_{23}). \end{aligned} \quad (49)$$

Now we evaluate

$$\begin{aligned} \langle D^2 \rangle &= \langle (\mathbf{k}^a \cdot \mathbf{X}_a)^2 \rangle = \langle (\mathbf{k}_1 \cdot \mathbf{X}_{13} + \mathbf{k}_2 \cdot \mathbf{X}_{23})^2 \rangle \\ &= \frac{1}{2} k_1^2 \Gamma(\sigma_{13}) + \frac{1}{2} k_2^2 \Gamma(\sigma_{23}) + \mathbf{k}_1 \cdot \mathbf{k}_2 \langle \mathbf{X}_{13} \cdot \mathbf{X}_{23} \rangle. \end{aligned} \quad (50)$$

It can be shown that

$$\langle \mathbf{X}_{13} \cdot \mathbf{X}_{23} \rangle = \frac{1}{2} [\Gamma(\sigma_{13}) + \Gamma(\sigma_{23}) - \Gamma(\sigma_{12})], \quad (51)$$

hence

$$\begin{aligned} \langle D^2 \rangle &= -\frac{1}{2} [\mathbf{k}_1 \cdot \mathbf{k}_3 \Gamma(\sigma_{13}) + \mathbf{k}_2 \cdot \mathbf{k}_3 \Gamma(\sigma_{23}) \\ &+ \mathbf{k}_1 \cdot \mathbf{k}_2 \Gamma(\sigma_{12})]. \end{aligned} \quad (52)$$

Note that this expression is symmetric under the interchange of any pair $\{\sigma_a, \sigma_b\}$ and $\{\mathbf{k}_a, \mathbf{k}_b\}$. Contracting Eq. (44) with $k_1^A k_2^B k_3^C$, and defining

$$\kappa_{ab} \equiv -\mathbf{k}_a \cdot \mathbf{k}_b, \quad (53)$$

we have

$$\begin{aligned} B(\mathbf{k}_1, \mathbf{k}_2, \mathbf{k}_3) &= -\epsilon^3 \frac{1}{\mathcal{A}} \frac{1}{4k_1^2 k_2^2 k_3^2} \int d\sigma_1 d\sigma_2 d\sigma_3 \\ &\times \left\{ \kappa_{12} [\kappa_{13} \Pi(\sigma_{13}) + \kappa_{23} \Pi(\sigma_{23})] V(\sigma_{12}) \right. \\ &+ \kappa_{13} [\kappa_{12} \Pi(\sigma_{12}) + \kappa_{23} \Pi(\sigma_{32})] V(\sigma_{31}) \\ &+ \left. \kappa_{23} [\kappa_{12} \Pi(\sigma_{21}) + \kappa_{13} \Pi(\sigma_{31})] V(\sigma_{23}) \right\} \\ &\times \exp \left\{ -\frac{1}{4} [\kappa_{13} \Gamma(\sigma_{13}) + \kappa_{23} \Gamma(\sigma_{23}) + \kappa_{12} \Gamma(\sigma_{12})] \right\}. \end{aligned} \quad (54)$$

We perform the integrations over the string coordinates σ_a in the Appendix A, where it is found

$$\begin{aligned} B(\mathbf{k}_1, \mathbf{k}_2, \mathbf{k}_3) &= -\epsilon^3 \pi c_0 \frac{\bar{v}^2 L \hat{\xi}}{\bar{t}^4 \mathcal{A} \hat{\xi}^2} \frac{1}{k_1^2 k_2^2 k_3^2} \\ &\times \left[\frac{k_1^4 \kappa_{23} + k_2^4 \kappa_{31} + k_3^4 \kappa_{12}}{(\kappa_{23} \kappa_{31} + \kappa_{12} \kappa_{31} + \kappa_{12} \kappa_{23})^{3/2}} \right] \end{aligned} \quad (55)$$

This is our primary expression for the bispectrum induced by the GKS effect in cosmic strings. It is proportional to $(GU)^3$, and therefore goes as the 3/2 power of the power spectrum. The factor $L \hat{\xi} / \mathcal{A}$ is a geometrical factor of order unity, as the projected string length per unit area is of order the projected correlation length $\hat{\xi}$ (unless there are a large number string networks which do not interact with each other). The factor in curly brackets is geometrical in Fourier space, depending on the relative lengths and angles of the \mathbf{k}_a . The overall dependence on angular quantities is therefore $\hat{\xi}^{-2} k^{-6}$. The dependence on string correlators appears through \bar{t} , \bar{v}^2 , and c_0 defined in Eqs. (22) to (25). This last is an interesting quantity as it is not time-reversal invariant: hence the bispectrum could vanish only if the string network is time symmetric. In an expanding universe, the existence of an asymmetry is ensured by decay of the string network. It was argued at the end of Section IIC that c_0 should be positive.

F. Comparison with data

Current analysis of the CMB temperature bispectrum focus essentially on a particular local model of primordial non-Gaussianity as well as specific configurations of the bispectrum wavenumbers. From Eq. (55), we can nevertheless estimate the string induced bispectrum for various symmetrical triangle configurations in Fourier space.

1. Equilateral triangle

In the case of \mathbf{k}_a arranged in an equilateral triangle such that

$$|\mathbf{k}_1| = |\mathbf{k}_2| = |\mathbf{k}_3| = k, \quad (56)$$

one has $\kappa_{ab} = k^2/2$, and the factor in the squared brackets in Eq. (55) becomes $4/\sqrt{3}$. As the result,

$$B_{kkk} \equiv B_{\text{eq}}(\mathbf{k}_1, \mathbf{k}_2, \mathbf{k}_3) = -\epsilon^3 \frac{4\pi}{\sqrt{3}} c_0 \frac{\bar{v}^2 L \hat{\xi}}{t^4 \mathcal{A}} \frac{1}{\hat{\xi}^2 k^6}. \quad (57)$$

With $c_0 > 0$, such a configuration produces a negative bispectrum decaying as $1/k^6$. We can estimate the size of the equilateral bispectrum from strings if they contribute about 10% of the temperature power spectrum at $\ell = 10$, in which case $\epsilon \simeq 2 \times 10^{-5}$, assuming Abelian Higgs strings where $GU \simeq 0.7 \times 10^{-6}$ [13, 29]:

$$B_{kkk} \simeq -(4 \times 10^{-14}) c_0 \frac{\bar{v}^2 L \hat{\xi}}{t^4 \mathcal{A}} \frac{1}{\hat{\xi}^2 k^6} \left(\frac{GU}{0.7 \times 10^{-6}} \right)^3. \quad (58)$$

It is not easy to compare with existing estimates as much of the literature focuses on a particular local model of primordial non-Gaussianity in which the Newtonian potential is parametrised

$$\Phi(\mathbf{x}) = \Phi(\mathbf{x})_{\text{L}} + f_{\text{NL}} [\Phi_{\text{L}}^2(\mathbf{x}) - \langle \Phi_{\text{L}}^2(\mathbf{x}) \rangle]. \quad (59)$$

With COBE-normalised CMB temperature fluctuations, and neglecting Silk damping, Ref. [30] gives the estimate

$$B_{lll} \simeq (2 \times 10^{-17}) l^{-4} f_{\text{NL}}. \quad (60)$$

String fluctuations would therefore appear to correspond to a f_{NL} of around -10^3 at $k\hat{\xi} \simeq 1$, which one can estimate to be near the peak of the scalar modes at $\ell \sim 500$. This number should be considered as an order of magnitude estimate since the string bispectrum calculation is only accurate for higher ℓ , while Eq. (60) is applicable for $\ell \leq 1000$ [30]. Notice that such a value for f_{NL} quickly drops with ℓ below WMAP detection limits [31].

2. Isosceles triangle

We now consider isosceles triangle configurations in Fourier space such that

$$|\mathbf{k}_1| = |\mathbf{k}_2| = k, \quad |\mathbf{k}_3| = 2k \sin \frac{\theta}{2}, \quad (61)$$

where θ denotes the angle between the wavevectors \mathbf{k}_1 and \mathbf{k}_2 . The cross scalar products simplify to

$$\kappa_{12} = k^2 \cos \theta, \quad \kappa_{23} = \kappa_{31} = 2k^2 \sin^2(\theta/2), \quad (62)$$

and the isosceles bispectrum reads

$$B_{\text{iso}}(k, \theta) = -\epsilon^3 \pi c_0 \frac{\bar{v}^2 L \hat{\xi}}{t^4 \mathcal{A}} \frac{1}{\hat{\xi}^2 k^6} \frac{1 + 4 \cos \theta \sin^2(\theta/2)}{\sin^3 \theta}. \quad (63)$$

It is immediate to check that for $\theta = \pi/3$, we recover Eq. (57). In Fig. 2, we have plotted the angle dependency of the isosceles bispectrum. Such a configuration diverges in the two flat triangle limits for which either $\theta \rightarrow 0$ or

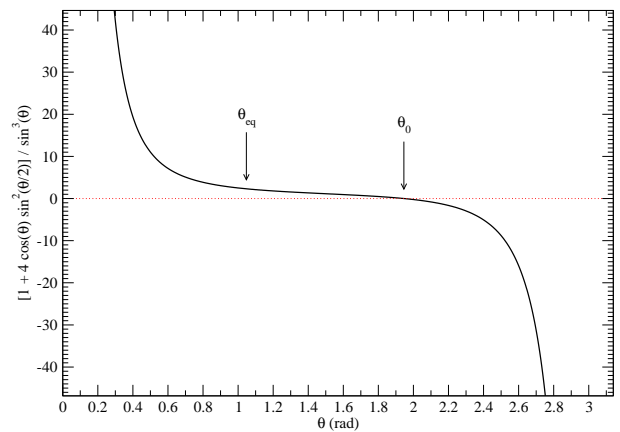


FIG. 2: Angular dependency of the isosceles bispectrum as a function of the angle θ in between the wavevectors \mathbf{k}_1 and \mathbf{k}_2 . The particular values $\theta_{\text{eq}} = \pi/3$ corresponding to the equilateral configuration as θ_0 at which the bispectrum vanishes are represented. Notice the divergences for flat triangle configurations at $\theta \rightarrow 0$ (squeezed) and $\theta \rightarrow \pi$ (collapsed).

$\theta \rightarrow \pi$. Both of these configurations are therefore better suited than the equilateral one to characterize the strings. Notice also the change of sign which occurs for the angle

$$\theta_0 = 2 \arccos \frac{\sqrt{3} - \sqrt{3}}{2}. \quad (64)$$

For $\theta < \theta_0$, one has $B_{\text{iso}} < 0$ (as for example in the equilateral configuration), whereas for $\theta > \theta_0$ the bispectrum $B_{\text{iso}} > 0$.

3. Squeezed triangles

This is the case of one of the sides of the triangle vanishing $k_3 \rightarrow k\theta$, with the opposite angle $\theta \rightarrow 0$. The angular factor in Eq. (63) simplifies to $1/\theta^3$ and

$$B_{kk\theta} \equiv \lim_{\theta \rightarrow 0} B_{\text{iso}}(k, \theta) \underset{\theta \rightarrow 0}{\sim} -\epsilon^3 \pi c_0 \frac{\bar{v}^2 L \hat{\xi}}{t^4 \mathcal{A}} \frac{1}{\hat{\xi}^2 k^6} \frac{1}{\theta^3}. \quad (65)$$

The bispectrum is therefore negative and appears to diverge in the squeezed limit. In practice, it is not possible to observe such a divergence as the maximum value of the wave vector is bounded by the detector resolution, and the minimum by the map size. Let us also recap that the above calculation breaks down at low wave numbers, and thus for the too small values of θ , since the GKS effect would no longer be the dominant source of temperature anisotropies. It is unclear at what ℓ this happens, but we note that there is no sign of an ℓ^{-1} power law in [32], so the GKS effect may be a subdominant contribution to the cosmic string power spectrum for $\ell < 1500$.

4. Collapsed triangles

There is however another flat triangle configuration for which all wavenumbers scale similarly. For $\theta \rightarrow \pi$, we have a collapsed triangle with $k_1 = k_2 = k$ and $k_3 \rightarrow 2k$. Denoting by

$$\varphi \equiv \pi - \theta, \quad (66)$$

the isosceles bispectrum reduces to

$$B_{k\varphi\varphi} \equiv \lim_{\theta \rightarrow \pi} B_{\text{iso}}(k, \theta) \underset{\varphi \rightarrow 0}{\sim} +\epsilon^3 3\pi c_0 \frac{\bar{v}^2 L \hat{\xi}}{t^4} \frac{1}{\mathcal{A}} \frac{1}{\xi^2 k^6} \frac{1}{\varphi^3}. \quad (67)$$

Notice the divergence but with a positive bispectrum. Again, such a divergence is not observable in a realistic situation due to the finite detector resolution. Nevertheless, flat triangles should provide a better framework for the search of a string bispectrum signature. In fact, the change of sign in between the squeezed and collapsed triangles is also of interest to improve the signal to noise ratio. Subtracting these two configurations with the appropriate angles should enhance the string signal over the noise.

III. NUMERICAL ESTIMATE

In this section, we directly compute the three point function in Fourier space from a set of 300 CMB temperature maps induced by cosmic strings in the flat sky approximation. These maps have been obtained along the lines of Ref. [21] from Nambu–Goto numerical simulations in FLRW space-time. As detailed in this reference, they are obtained from the GKS effect using Eq. (4), and are therefore valid on small angular scales only. In the next sections, we briefly recall the numerical method used to generate the maps and then discuss our bispectrum estimator.

A. Nambu–Goto numerical simulations

Our FLRW numerical simulations are based on an improved version of the Bennett and Bouchet Nambu-Goto cosmic string code [21, 33, 34]. The runs are performed in a comoving box with periodic boundary conditions and whose volume has been scaled to unity. The horizon size d_{h_0} is a free parameter controlling the initial string energy within a horizon volume. For the simulations we performed, $d_{\text{h}_0} \simeq 0.185$. The string network is assumed to come from Vachaspati-Vilenkin initial conditions for which the long strings path is a random walk of correlation length ℓ_c , plus a random transverse velocity component of root mean squared amplitude 0.1 [35]. These parameters are set as in Ref. [21] to minimize the relaxation time of the Vachaspati-Vilenkin string network

toward its stable cosmological configuration. The temperature maps are then produced according the GKS effect generated by the strings intercepting our past light cone, using the Eq. (4)

$$\Theta \simeq \frac{8\pi i GU}{k^2} \int_{\mathbf{X} \cap \mathbf{x}_\gamma} (\mathbf{u} \cdot \mathbf{k}) e^{-i\mathbf{k} \cdot \mathbf{X}} e^{-\tau} \epsilon d\sigma, \quad (68)$$

where $\tau(\mathbf{X})$ is the optical depth to the position of the string, along the line of sight $\hat{\mathbf{n}}$, and

$$\mathbf{u} = \dot{\mathbf{X}} - \frac{(\hat{\mathbf{n}} \cdot \dot{\mathbf{X}}') \cdot \dot{\mathbf{X}}'}{1 + \hat{\mathbf{n}} \cdot \dot{\mathbf{X}}}. \quad (69)$$

The cosmic string simulations are used to compute \mathbf{u} , based on the string trajectories \mathbf{X} . The map generation procedure introduces one additional parameter which is the redshift at which we start the simulations z_i . It has been set to the last scattering surface, namely $z_i = 1089$, and in a flat Λ CDM universe, using fiducial values for the density parameters compatible with the three-year Wilkinson Microwave Anisotropy Probe (WMAP) data [36], this corresponds to a numerical comoving box of $L_{\text{sim}} \simeq 1.7$ Gpc. Such a size subtends an angle of $\theta_{\text{fov}} \simeq 7.2^\circ$ in the sky. The Nambu-Goto simulations and the associated CMB maps therefore depend on only two parameters: the string energy per unit length U , and the initial correlation length ℓ_c . The dependence on ℓ_c should drop out at late times, as the network is believed to approach a self-similar or scaling configuration. However, in a real Nambu-Goto simulation, there is still some non-scaling structure evident on the smallest length scales [21]. As an illustration example, a typical CMB temperature anisotropy map is represented in Fig. 3, together with the seeding strings projected on our past light cone. We have used our numerical simulations to create 300 statistically independent temperature maps from which one can construct a bispectrum estimator.

B. Reduced bispectrum estimator

1. Scale convolution method

The bispectrum computations use the scale convolution method introduced in Ref. [23] and applied to the flat sky approximation in Ref. [37]. This method relies on the choice of unity window functions in Fourier space $W_u(k)$ peaked around a particular wavenumber u . Defining

$$\Theta_u(\mathbf{x}) \equiv \int \frac{d\mathbf{k}}{(2\pi)^2} \hat{\Theta}_{\mathbf{k}} W_u(k) e^{-i\mathbf{k} \cdot \mathbf{x}}, \quad (70)$$

one can construct an estimator of the three point function in Fourier space by remarking that

$$\int \Theta_{k_1}(\mathbf{x}) \Theta_{k_2}(\mathbf{x}) \Theta_{k_3}(\mathbf{x}) d\mathbf{x} = \int \frac{d\mathbf{p} d\mathbf{q} d\mathbf{k}}{(2\pi)^6} \hat{\Theta}_{\mathbf{p}} \hat{\Theta}_{\mathbf{q}} \hat{\Theta}_{\mathbf{k}} \times W_{k_1}(p) W_{k_2}(q) W_{k_3}(k) (2\pi)^2 \delta(\mathbf{p} + \mathbf{q} + \mathbf{k}). \quad (71)$$

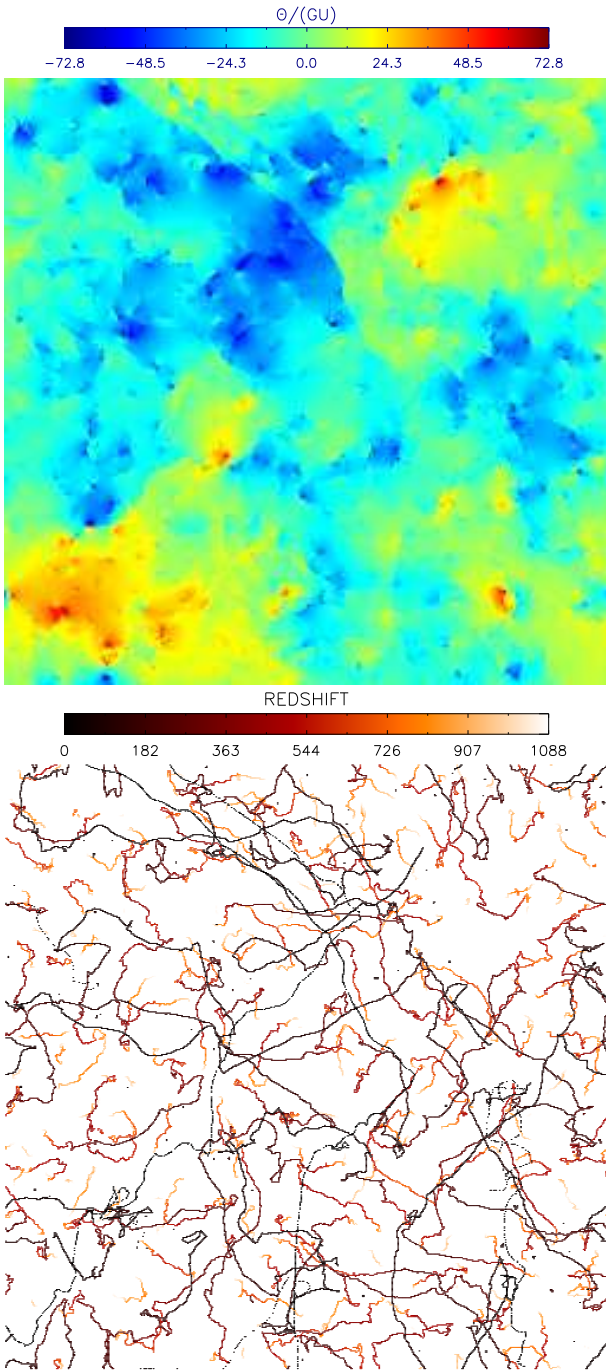


FIG. 3: Typical CMB temperature map on a 7.2° field (resolution of $\theta_{\text{res}} = 0.42'$, $n_{\text{pix}}^2 = 1024^2$) obtained from Nambu-Goto cosmic string simulations (upper panel). The lower panel traces back the strings projected on our past light cone.

For peaked enough window functions, $\hat{\Theta}_{\mathbf{k}}$ remains constant over the window functions width and we construct our reduced bispectrum estimator as

$$b_{k_1 k_2 k_3} = \frac{1}{S_{k_1 k_2 k_3}^{(w)}} \left\langle \int \Theta_{k_1}(\mathbf{x}) \Theta_{k_2}(\mathbf{x}) \Theta_{k_3}(\mathbf{x}) d\mathbf{x} \right\rangle. \quad (72)$$

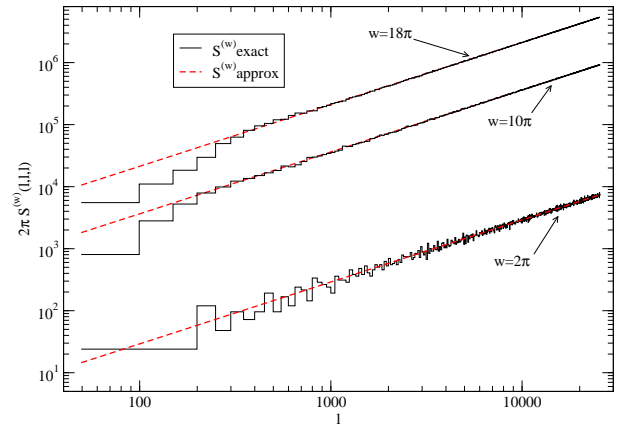


FIG. 4: Exact versus approximated geometrical $S_{\ell\ell\ell}^{(w)}$ factors for a map with 1024^2 pixels and various choices of the window function with w ($w = 2\pi$ corresponds to one Fourier mode per bandwidth). For large values of w , the deviations for the small multipoles come from the averaging effect. For small angles we are interested in, Eq. (75) provides a good approximation to the exact expression (73).

where the function $S^{(w)}$ is the flat sky equivalent of the inverse Wigner-3j symbols and reads

$$S_{k_1 k_2 k_3}^{(w)} = \int \frac{d\mathbf{p}d\mathbf{q}}{(2\pi)^4} W_{k_1}(\mathbf{p}) W_{k_2}(\mathbf{q}) W_{k_3}(\mathbf{p} + \mathbf{q}). \quad (73)$$

As noted in Ref. [37], S is of geometrical nature and needs to be computed only once. However, at small angular scales, S is generically a four-dimensional integral whose computation can be time consuming for the large wavenumbers. For thin enough window functions, it is nevertheless possible to derive an analytical approximation. Assuming that $W_u(k) = 1$ for $u - w/2 < k < u + w/2$, and zero otherwise, for small enough width w one has

$$W_u(k) \simeq w\delta(k - u). \quad (74)$$

With \mathbf{k}_1 , \mathbf{k}_2 and \mathbf{k}_3 forming a triangle, Eq. (73) can be exactly integrated and one finds

$$S^{(w)} \simeq \left(\frac{w}{2\pi}\right)^3 \frac{4k_1 k_2 k_3}{\sqrt{[(k_1 + k_2)^2 - k_3^2][k_3^2 - (k_1 - k_2)^2]}}. \quad (75)$$

As can be checked in Fig. 4, the analytical approximation of $S_{k_1 k_2 k_3}^{(w)}$ given in Eq. (75) is particularly accurate for the large wavenumbers. This approach ends up being numerically convenient since it requires only three Fourier transforms to compute the $\Theta_{\mathbf{k}}(\mathbf{x})$, together with an integration over all map pixels.

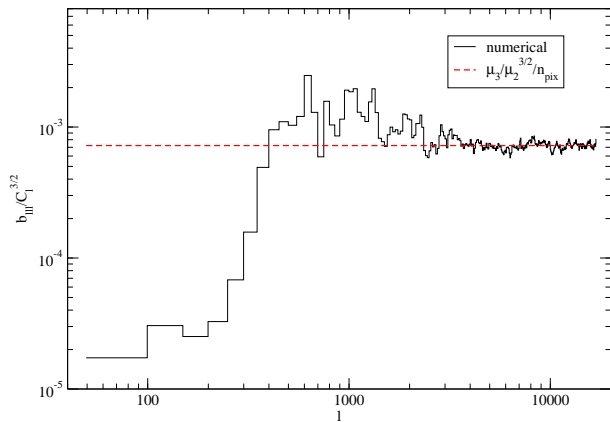


FIG. 5: The reduced bispectrum computed by the scale convolution method and averaged over a hundred of non-Gaussian synthetic LCDM temperature maps whose probability distribution function is given by Eq. (76). The red dashed line is the expected non-Gaussian signal. The missing power for low multipoles comes from the cutoff at $\ell_w \simeq w/\theta_{\text{fov}}$ introduced by the choice of large w values for the window functions.

2. Statistical averaging and numerical tests

From the previous discussion, the bispectrum is extracted and averaged over the 300 statistical independent maps and for the various triangle configurations discussed in Sect. II F. Our results are presented in the next section. The variance of the bispectrum over the different maps is used to provide an estimate of the statistical errors associated with our approach. Notice however, as discussed at length in Ref. [21], the Nambu-Goto string simulation do also lead to some systematic errors due to the non-scaling structure. This can be greatly reduced by eliminating some of the small loops from the network. In order to check our numerical bispectrum estimator, we have performed two tests. The first was to generate a set of synthetic non-Gaussian CMB temperature maps from the non-Gaussian probability distribution

$$P_{\alpha,\sigma}(\Theta) = \frac{e^{-\Theta^2/(2\sigma^2)}}{\sqrt{2\pi}\sigma} \left[\sqrt{1-\alpha^2} + \frac{\alpha}{\sqrt{48}} H_3 \left(\frac{\Theta}{\sqrt{2}\sigma} \right) \right], \quad (76)$$

where H_3 stands for the third Hermite polynomial. As shown in Ref. [38, 39], such a statistics leads to a reduced bispectrum whose amplitude is given

$$\frac{b_{\ell_1\ell_2\ell_3}}{\sqrt{C_{\ell_1}C_{\ell_2}C_{\ell_3}}} = \frac{1}{n_{\text{pix}}} \frac{\mu_3}{\mu_2^{3/2}}, \quad (77)$$

where $\mu_2 = \sigma^2(1 + 6\alpha^2)$ and $\mu_3 = (2\sigma^2)^{3/2}\alpha\sqrt{3(1-\alpha^2)}$ are the second and third central moment, respectively. It is not difficult to show that $\mu_3/\mu_2^{3/2}$ is maximised for $\alpha^2 = (7 - \sqrt{43})/6$. In Fig. 5, we have plotted the bispectrum obtained from the scale convolution method averaged over a hundred of such non-Gaussian LCDM temperature maps together with its analytical expectation.

At small scales, and up to the statistical errors, the non-Gaussian signal is recovered with the right amplitude. Notice that the loss of power for the low multipoles is simply an artifact coming from the choice of a large window function width ($w = 52\pi$). This necessarily introduces a lower frequency cutoff around $\ell_w \simeq w/\theta_{\text{fov}}$, and also close to the Nyquist frequency (not visible on the plots). As discussed in the following, increasing the values of w reduces the variance of the bispectrum estimator² at the price of losing information for the lower multipoles and those close to the Nyquist frequency. The second test we have performed is to integrate the cosmic string bispectrum over all possible triangle configurations such as to check that we indeed recover the skewness of the string temperature anisotropies. Averaged over the 300 string maps, we find the mean sample skewness to be negative

$$g_1 \equiv \left\langle \frac{(\Theta - \bar{\Theta})^3}{\sigma^3} \right\rangle \simeq -0.22 \pm 0.12, \quad (78)$$

where the brackets stand for the mean over different realisations while the bar denotes averaging on each map. The variance itself averages to

$$\sigma^2 = \left\langle (\Theta - \bar{\Theta})^2 \right\rangle \simeq (150.7 \pm 18) (GU)^2. \quad (79)$$

The quoted errors are statistical and refer to the square root of the variance between the different realisations.

C. Equilateral configurations

The previously described method has been applied to extract the equilateral bispectrum $b_{\ell\ell\ell}$. In Fig. 6, we have plotted its mean value over the 300 different maps as well as its standard deviation. To reduce the variance of the estimator we have chosen $w = 30\pi$ which gives a low multipole cutoff $\ell_w \simeq 750$. The equilateral bispectrum decays faster than its standard deviation at the large multipoles which renders its numerical determination challenging.

It is however clear from this plot that $b_{\ell\ell\ell} < 0$ in agreement with the analytical results of Sect. II. A power law fit against the mean numerical estimator over the range of multipoles $\ell_w < \ell < \ell_{\text{max}}$, with $\ell_{\text{max}} = 16000$ gives

$$[\ell(\ell+1)]^{3/2} b_{\ell\ell\ell} \underset{\ell \gg 1}{\propto} \ell^{-q} \quad \text{with } q = 2.82. \quad (80)$$

We do not quote error bars since this value is relatively sensitive to the choice of ℓ_{max} and, as can be seen in Fig. 6, the standard deviation of our estimator becomes an order of magnitude bigger than the bispectrum itself for $\ell > 16000$. The power dependency of Eq. (80) is

² Simply by increasing the number of equivalent triangle configurations in Fourier space probed by the window functions.

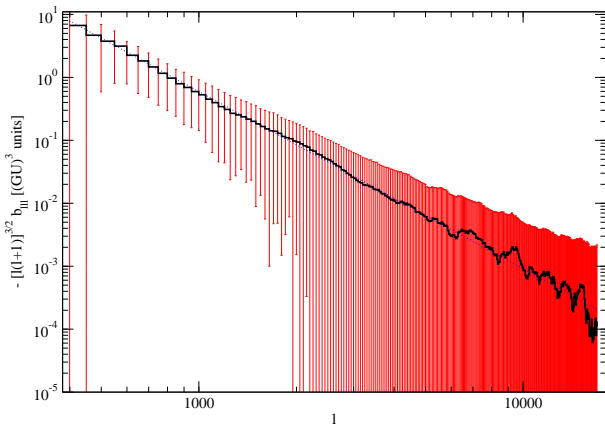


FIG. 6: Mean and standard deviation of the equilateral bispectrum $[\ell(\ell+1)/(2\pi)]^{3/2} b_{\ell\ell\ell}$ over our 300 string temperature maps and obtained for window function width $w = 30\pi$. The blue dotted line is the power law fit of Eq. (80).

however remarkably close to the analytical expectation. In fact, the non-integer value for the power may be expected due to the fractal properties of the Nambu–Goto strings [20]. As shown in Ref. [21], the power spectrum itself was found to behaves as

$$\ell(\ell+1)C_\ell \underset{\ell \gg 1}{\propto} \ell^{-p} \quad \text{with } p = 0.889. \quad (81)$$

From Eqs. (80) and (81), we find the analytical power law behaviour of the ratio

$$\frac{b_{\ell\ell\ell}}{C_\ell^{3/2}} \underset{\ell \gg 1}{\propto} \ell^{-(q-3p/2)} \quad \text{with } q - \frac{3}{2}p = 1.49. \quad (82)$$

Concerning the overall amplitude, we find at $\ell = 1000$

$$[\ell(\ell+1)/(2\pi)]^{3/2} b_{\ell\ell\ell} \simeq (-0.53 \pm 0.3) (GU)^3, \quad (83)$$

which is again of the same order of magnitude as our analytical estimate.

In order to understand the increase of the standard deviation at small scales, one can use the nearly Gaussian approximation in which the non-Gaussian trispectrum is neglected. Under these assumptions, the variance of the bispectrum estimator is given by [37, 40]

$$\sigma_b^2 = \frac{6}{S_{\ell\ell\ell}^{(w)}} C_\ell^3. \quad (84)$$

Using Eq. (75), one gets

$$\sigma_b = \sqrt{\frac{2\pi}{\theta_{\text{fov}}}} \left(\frac{2\pi}{w}\right)^{3/2} \left[\frac{27}{4\ell(\ell+1)}\right]^{1/4} \left[\frac{\ell(\ell+1)C_\ell}{2\pi}\right]^{3/2}. \quad (85)$$

As expected, the variance is reduced by a factor w^3 coming from the different numbers of equivalent triangle configurations probed by window functions of width

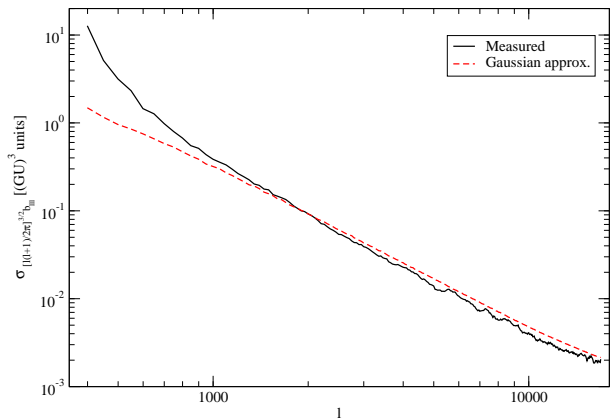


FIG. 7: Standard deviation of the bispectrum estimator over the 300 string temperature maps (black solid curve) compared with the nearly Gaussian random expected standard deviation obtained from Eq. (85).

w . From Eqs. (81) and (85), one gets $\sigma_b \propto \ell^{-4.83}$ which vanishes slower than the bispectrum estimator at large multipoles. In Fig. 7, we have plotted the standard deviation obtained from Eq. (85), and relying only on the mean string power spectrum, together with the measured standard deviation of our bispectrum estimator. There is good agreement for both the power law behaviour and the overall amplitude. From this section, we conclude that although the cosmic string equilateral bispectrum is non-vanishing, its measurement at small angles may be difficult due to its fast decay compared to the associated standard deviation. We have however confirmed the analytical results of Sect. II, up to the non-integer power law value which may be interpreted as a fractal effect associated with the Nambu–Goto string small scale structure. As we discuss in the next section, other triangle configurations are better suited for the search of cosmic string bispectrum in the CMB temperature anisotropies.

D. Flat triangle configurations

1. Squeezed triangle

Let us first consider the triangle configuration in the squeezed limit such that

$$k_1 = k_2 = k, \quad k_3 \simeq k\theta, \quad (86)$$

that we refer to as “ $\ell\ell\theta$ ”. The mean value of $b_{\ell\ell\theta}$ over the different maps have been plotted in Fig. 8 and for various values of the squeezed angle θ . As found analytically, the overall amplitude is found to be enhanced by a factor $1/\theta^3$, rendering its numerical determination much easier than its equilateral analogous. As a result, the width of the window function has been kept to a lower value, namely $w = 10\pi$ for this plot. However, due to the finite field of view, we cannot go to

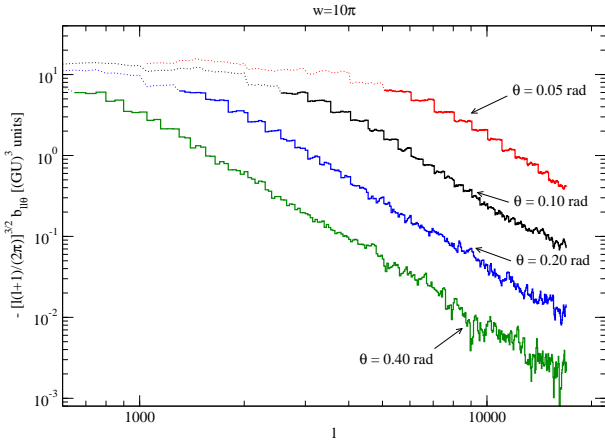


FIG. 8: Squeezed angle dependency of the mean squeezed bispectrum $[\ell(\ell+1)/(2\pi)]^{3/2} b_{\ell\ell\theta}$. The spurious plateau (dotted lines) for the lower multipoles comes from the cutoff associated with a given squeezed angle θ together with the window function width w : $\ell_{\min} = w/(\theta_{\text{fov}}\theta)$.

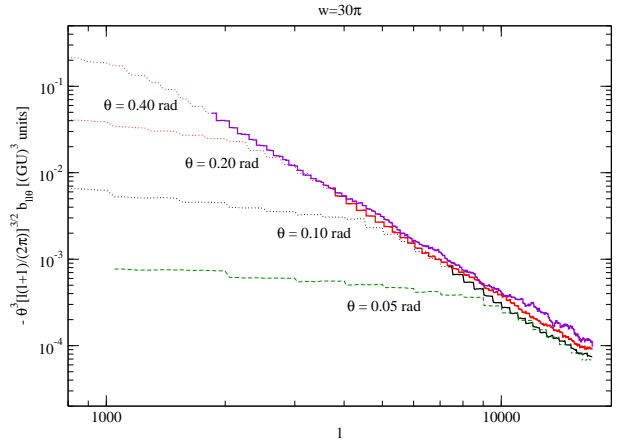


FIG. 10: Rescaled mean squeezed bispectrum $\theta^3[\ell(\ell+1)/(2\pi)]^{3/2} b_{\ell\ell\theta}$ showing the $1/\theta^3$ dependency. Notice the large window function width $w = 30\pi$ chosen to reduce the statistical errors and pushing up the numerical multipole cutoff.

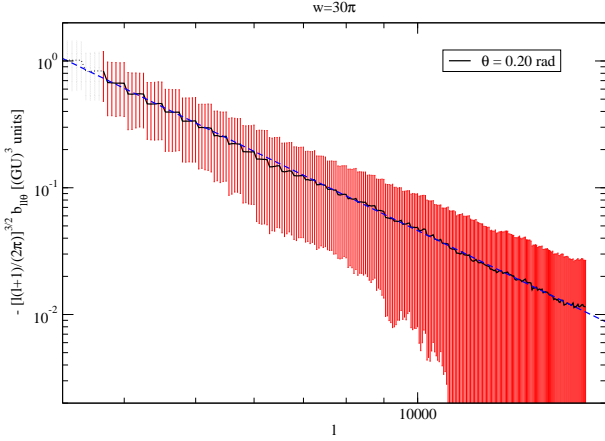


FIG. 9: Mean value and standard deviation of the squeezed bispectrum $[\ell(\ell+1)/(2\pi)]^{3/2} b_{\ell\ell\theta}$ for $\theta = 0.2$ radians. The window function width has been increased to $w = 30\pi$ to reduce the variance pushing up the lower multipole cutoff to $\ell_{\min} = w/(\theta_{\text{fov}}\theta) \simeq 3750$. The dashed line is the best power law fit whose power has been set to the one obtained from the equilateral configuration [see Eq. (80)].

very small squeezed angle without truncating the lower modes. From Eq. (86), the lowest multipole achievable is therefore given by $\ell_{\min} = w/(\theta_{\text{fov}}\theta)$, where the window function cutoff has been considered. In order to compare the power law behaviour of the squeezed and equilateral configuration, we have plotted in Fig. 9, the mean value and standard deviation of the squeezed bispectrum for the particular angle $\theta = 0.2$ radians. The variance has been reduced as far as we could by using a large window function width $w = 30\pi$. This explains the low multipole cutoff at a quite large value of $\ell_{\min} \simeq 3750$. A power

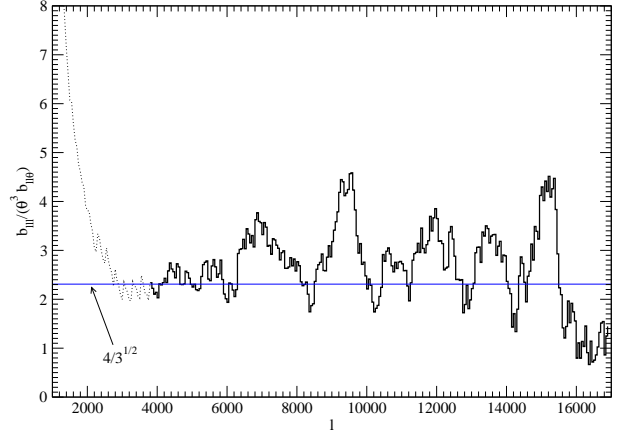


FIG. 11: Ratio of the mean bispectra $b_{\ell\ell\ell}/(\theta^3 b_{\ell\ell\theta})$ obtained for $\theta = 0.2$ radians. Up to the statistical errors, the expected value $4/\sqrt{3}$ is recovered for $\ell > \ell_{\min}$.

law fit for $\ell > \ell_{\min}$ gives the same power value as the one obtained for the equilateral bispectrum in Eq. (80). The dashed blue line in Fig. 9 is the best power law fit ℓ^{-q} . The $1/\theta^3$ dependency of the squeezed bispectrum is illustrated in Fig. 10. Again, to reduce the variance, the width has been set to $w = 30\pi$ and we have plotted $\theta^3[\ell(\ell+1)/(2\pi)]^{3/2} b_{\ell\ell\theta}$ for the four θ values of Fig. 8. As expected, all rescaled mean values match above their respective multipole cutoff ℓ_{\min} . Concerning the overall amplitude, it can be evaluated around the minimum variance multipole and we find at $\ell = 5000$

$$[\ell(\ell+1)/(2\pi)]^{3/2} b_{\ell\ell\theta} \simeq (-2.7 \pm 1.4) \times 10^{-3} \left(\frac{GU}{\theta}\right)^3. \quad (87)$$

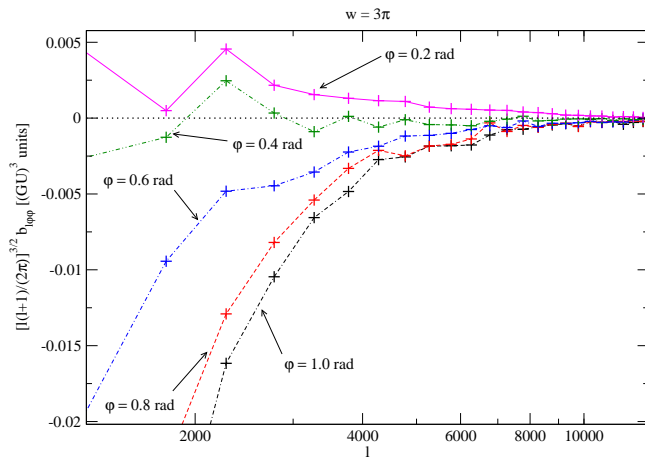


FIG. 12: Mean collapsed bispectrum $[\ell(\ell + 1)/(2\pi)]^{3/2} b_{\ell\varphi\varphi}$. This configuration is extremely sensitive to the window function properties and statistical errors dominate. The change of sign for small values of φ is nevertheless observable.

Using the power law fit, such an amplitude can be extrapolated down to $\ell = 1000$ and compared to Eq. (83). In particular, we recover, up to the statistical errors, the analytical result

$$\frac{b_{\ell\ell\ell}}{\theta^3 b_{\ell\ell\theta}} = \frac{4}{\sqrt{3}}. \quad (88)$$

For completeness, the above ratio has been plotted for $\theta = 0.2$ radians in Fig. 11. To conclude this section, the squeezed bispectrum is also found to follow the analytical results of Sect. II, again up to the non-integer power law behaviour with respect to the multipole moment.

2. Collapsed triangles

As discussed in Sect. II F 4, the collapsed triangles correspond to the limit $\varphi \rightarrow 0$ for the isosceles configuration and to the mode values

$$k_1 = k_2 = k, \quad k_3 \simeq 2k. \quad (89)$$

The scale convolution method is hardly applicable in this case since all collapsed triangles fitting in the window function width will be undistinguishable. Although this averaging effect allowed us to increase the statistics for the other triangle configurations, for the collapsed ones one cannot longer assume that the bispectrum is constant over the window function, especially since it diverges in the limit $\varphi \rightarrow 0$. As a result, w has been kept to a low value ($w = 3\pi$) and the modes have been binned to reduce the statistical errors. As can be seen in Fig. 12, our numerical estimation does not allow to accurately traces the bispectrum down to the small values of φ . Nevertheless, we do observe the change of sign for $\varphi \rightarrow 0$ albeit at a smaller values than the one predicted analytically.

IV. CONCLUSION

We have analytically and numerically derived the CMB temperature bispectrum induced by cosmic strings from the Gott–Kaiser–Stebbins effect. This effect is the main source of string induced CMB anisotropies at small angle and our result is applicable at those angular scales only. The bispectrum is negative for equilateral and all isosceles squeezed configuration, having a power law decay close to ℓ^{-6} . The squeezed isosceles bispectrum is significantly amplified for small squeezing angle by a factor θ^{-3} . Although the vanishing limit is forbidden by any finite detector resolution, one should expect the ongoing and future high resolution CMB experiment to be more sensitive to these signatures [41, 42, 43]. The collapsed isosceles configuration still exhibits the same power law, an angle dependency in φ^{-3} (with $\varphi = \pi - \theta$) but leads to a positive bispectrum. This feature could allow an enhancement of the string signal by subtracting the bispectrum of these two configurations.

The numerically measured amplitudes have been given in the text and roughly correspond to a $f_{\text{NL}} \simeq -10^3$ at $\ell = 500$ for equilateral configurations. This number should be treated with caution as there are competing and correlated effects at this angular scale, notably acoustic oscillations; however, it certainly shows that this is an interesting angular scale to search for string non-gaussianity using simulations with fluid perturbations included.

Finally, as the power law dependence of the bispectrum variance may suggest, we should expect an even stronger non-gaussian signal from the cosmic string trispectrum and we leave its analysis for a forthcoming work.

Acknowledgments

This work is partially supported by the Belgian Federal Office for Scientific, Technical, and Cultural Affairs through the Inter-University Attraction Pole Grant No. P6/11. The cosmic string simulations have been performed thanks to computing support provided by the Planck-HFI processing center at the Institut d’Astrophysique de Paris.

APPENDIX A: STRING COORDINATE INTEGRATIONS

In this Appendix we perform the integrals over the string coordinates σ_a in the expression (55) for the bispectrum. We repeat the expressions for convenience:

$$B(\mathbf{k}_1, \mathbf{k}_2, \mathbf{k}_3) = -\epsilon^3 \frac{1}{\mathcal{A}} \frac{k_{1A} k_{2B} k_{3C}}{k_1^2 k_2^2 k_3^2} \int d\sigma_1 d\sigma_2 d\sigma_3 \langle C^{ABC} D \rangle e^{-\frac{1}{2} \langle D^2 \rangle}. \quad (A1)$$

where

$$\begin{aligned}
& k_{1A} k_{2B} k_{3C} \langle C^{ABCD} \rangle e^{-\frac{1}{2}(D^2)} = \\
& \frac{1}{4} \left\{ \kappa_{12} [\kappa_{13}\Pi(\sigma_{13}) + \kappa_{23}\Pi(\sigma_{23})] V(\sigma_{12}) \right. \\
& \quad + \kappa_{13} [\kappa_{12}\Pi(\sigma_{12}) + \kappa_{23}\Pi(\sigma_{32})] V(\sigma_{31}) \\
& \quad \left. + \kappa_{23} [\kappa_{12}\Pi(\sigma_{21}) + \kappa_{13}\Pi(\sigma_{31})] V(\sigma_{23}) \right\} \\
& \times \exp \left\{ -\frac{1}{4} [\kappa_{13}\Gamma(\sigma_{13}) + \kappa_{23}\Gamma(\sigma_{23}) + \kappa_{12}\Gamma(\sigma_{12})] \right\}
\end{aligned} \tag{A2}$$

Thanks to the symmetry identified earlier, there is essentially only one integral to do, as the six terms in Eq. (55) in are related by a permutation symmetry. We can define a function of three variables

$$\begin{aligned}
F(\kappa_{12}, \kappa_{23}, \kappa_{31}) &= \int d\sigma_1 d\sigma_2 d\sigma_3 \Pi(\sigma_{13}) V(\sigma_{12}) \\
&\times \exp \left\{ \frac{1}{4} [-\kappa_{31}\Gamma(\sigma_{13}) - \kappa_{23}\Gamma(\sigma_{23}) - \kappa_{12}\Gamma(\sigma_{12})] \right\},
\end{aligned} \tag{A3}$$

in terms of which

$$\begin{aligned}
& k_1^A k_2^B k_3^C \langle C^{ABCD} \rangle e^{-\frac{1}{2}(D^2)} = \frac{1}{4} \{ \\
& \quad \kappa_{12}\kappa_{31} F(\kappa_{12}, \kappa_{23}, \kappa_{31}) + \kappa_{12}\kappa_{23} F(\kappa_{12}, \kappa_{31}, \kappa_{23}) \\
& \quad + \kappa_{31}\kappa_{12} F(\kappa_{31}, \kappa_{23}, \kappa_{12}) + \kappa_{31}\kappa_{23} F(\kappa_{31}, \kappa_{12}, \kappa_{23}) \\
& \quad + \kappa_{23}\kappa_{12} F(\kappa_{23}, \kappa_{31}, \kappa_{12}) + \kappa_{23}\kappa_{31} F(\kappa_{23}, \kappa_{12}, \kappa_{31}) \}.
\end{aligned} \tag{A4}$$

A change of coordinates simplifies the integration:

$$\sigma_{123} = \frac{1}{3}(\sigma_1 + \sigma_2 + \sigma_3), \tag{A5}$$

giving

$$\begin{aligned}
F(\kappa_{12}, \kappa_{23}, \kappa_{31}) &= \int d\sigma_{123} d\sigma_{12} d\sigma_{31} \Pi(\sigma_{31}) V(\sigma_{12}) \\
&\times \exp \left\{ \frac{1}{4} [-\kappa_{31}\Gamma(\sigma_{31}) - \kappa_{23}\Gamma(\sigma_{23}) - \kappa_{12}\Gamma(\sigma_{12})] \right\},
\end{aligned} \tag{A6}$$

where we have used $\Pi(\sigma_{31}) = \Pi(\sigma_{13})$ and $\Gamma(\sigma_{31}) = \Gamma(\sigma_{13})$. Inserting the identity

$$1 = \int d\sigma_{23} \delta(\sigma_{23} + \sigma_{12} + \sigma_{31}), \tag{A7}$$

and using an integral representation for the δ -function we have

$$\begin{aligned}
F(\kappa_{12}, \kappa_{23}, \kappa_{31}) &= L \int \frac{d\lambda}{2\pi} \int d\sigma_{12} d\sigma_{23} d\sigma_{31} \\
&\times \Pi(\sigma_{31}) V(\sigma_{12}) \exp [i\lambda(\sigma_{23} + \sigma_{12} + \sigma_{31})] \\
&\times \exp \left\{ -\frac{1}{4} [\kappa_{13}\Gamma(\sigma_{31}) + \kappa_{23}\Gamma(\sigma_{23}) + \kappa_{12}\Gamma(\sigma_{12})] \right\}.
\end{aligned} \tag{A8}$$

Hence we can factorise

$$F(\kappa_{12}, \kappa_{23}, \kappa_{31}) = L \int \frac{d\lambda}{2\pi} I(\lambda, \kappa_{12}) J(\lambda, \kappa_{23}) K(\lambda, \kappa_{31}), \tag{A9}$$

where

$$I(\lambda, \kappa_{12}) = \int d\sigma V(\sigma) e^{i\lambda\sigma - \frac{1}{4}\kappa_{12}\Gamma(\sigma)}, \tag{A10}$$

$$J(\lambda, \kappa_{23}) = \int d\sigma e^{i\lambda\sigma - \frac{1}{4}\kappa_{23}\Gamma(\sigma)}, \tag{A11}$$

$$K(\lambda, \kappa_{31}) = \int d\sigma \Pi(\sigma) e^{i\lambda\sigma - \frac{1}{4}\kappa_{31}\Gamma(\sigma)}. \tag{A12}$$

We evaluate I , J and K for small angles. For κ_{ab} large and positive, and assuming the relevant limits for the correlation functions

$$\Gamma(\sigma) \simeq \bar{t}^2 \sigma^2, \quad V(\sigma) \simeq \bar{v}^2, \quad \Pi(\sigma) \simeq \frac{1}{2} \frac{c_0}{\xi} \sigma^2, \tag{A13}$$

one gets

$$I(\lambda, \kappa_{12}) \simeq \frac{\bar{v}^2}{\bar{t}} \sqrt{\frac{4\pi}{\kappa_{12}}} \exp\left(-\frac{\lambda^2}{\kappa_{12}\bar{t}^2}\right), \tag{A14}$$

$$J(\lambda, \kappa_{23}) \simeq \frac{1}{\bar{t}} \sqrt{\frac{4\pi}{\kappa_{23}}} \exp\left(-\frac{\lambda^2}{\kappa_{23}\bar{t}^2}\right), \tag{A15}$$

$$K(\lambda, \kappa_{31}) \simeq \frac{c_0}{\xi} \frac{1}{\kappa_{31}\bar{t}^3} \sqrt{\frac{4\pi}{\kappa_{31}}} \left(1 - \frac{2\lambda^2}{\kappa_{31}\bar{t}^2}\right) \exp\left(-\frac{\lambda^2}{\kappa_{31}\bar{t}^2}\right). \tag{A16}$$

Hence

$$\begin{aligned}
F(\kappa_{12}, \kappa_{23}, \kappa_{31}) &\simeq 4\pi L \frac{\bar{v}^2}{\bar{t}^4} \frac{c_0}{\xi} \\
&\times \frac{\kappa_{23} + \kappa_{12}}{(\kappa_{23}\kappa_{31} + \kappa_{12}\kappa_{31} + \kappa_{12}\kappa_{23})^{3/2}}.
\end{aligned} \tag{A17}$$

Though we have assumed $\kappa_{ab} > 0$ in deriving this equation, the result is still applicable even if κ_{ab} is negative because the combination $\kappa_{23}\kappa_{31} + \kappa_{12}\kappa_{31} + \kappa_{12}\kappa_{23}$ in the denominator is positive definite. Actually, by using approximations (A13), one can derive (A17) directly from Eq. (A3) which is well-defined even for negative κ_{ab} because of the positive definiteness of the exponent. Defining the new function

$$g(\kappa_{12}, \kappa_{23}, \kappa_{31}) = \frac{\kappa_{12} + \kappa_{23}}{(\kappa_{23}\kappa_{31} + \kappa_{12}\kappa_{31} + \kappa_{12}\kappa_{23})^{3/2}}, \tag{A18}$$

we can write

$$\begin{aligned}
B(\mathbf{k}_1, \mathbf{k}_2, \mathbf{k}_3) &= -\epsilon^3 \pi c_0 \frac{\bar{v}^2}{\bar{t}^4} \frac{L\hat{\xi}}{\mathcal{A}} \frac{1}{\xi^2} \frac{1}{k_1^2 k_2^2 k_3^2} \\
&\times \left\{ \kappa_{12}\kappa_{31} g(\kappa_{12}, \kappa_{23}, \kappa_{31}) + \kappa_{12}\kappa_{23} g(\kappa_{12}, \kappa_{31}, \kappa_{23}) \right. \\
&\quad + \kappa_{31}\kappa_{12} g(\kappa_{31}, \kappa_{23}, \kappa_{12}) + \kappa_{31}\kappa_{23} g(\kappa_{31}, \kappa_{12}, \kappa_{23}) \\
&\quad \left. + \kappa_{23}\kappa_{12} g(\kappa_{23}, \kappa_{31}, \kappa_{12}) + \kappa_{23}\kappa_{31} g(\kappa_{23}, \kappa_{12}, \kappa_{31}) \right\}.
\end{aligned} \tag{A19}$$

Thanks to g being symmetric in its first two arguments, and using $\kappa_{23} + \kappa_{12} = k_2^2$ (and circular permutations), some simplification follows:

$$B(\mathbf{k}_1, \mathbf{k}_2, \mathbf{k}_3) = -\epsilon^3 \pi c_0 \frac{\bar{v}^2 L \hat{\xi}}{t^4 \mathcal{A}} \frac{1}{\hat{\xi}^2} \frac{1}{k_1^2 k_2^2 k_3^2} \times \left\{ \begin{aligned} &k_2^2 \kappa_{31} g(\kappa_{12}, \kappa_{23}, \kappa_{31}) + k_1^2 \kappa_{23} g(\kappa_{31}, \kappa_{12}, \kappa_{23}) \\ &+ k_3^2 \kappa_{12} g(\kappa_{23}, \kappa_{31}, \kappa_{12}) \end{aligned} \right\}. \quad (\text{A20})$$

Finally, using the definition of g from Eq. (A18),

$$B(\mathbf{k}_1, \mathbf{k}_2, \mathbf{k}_3) = -\epsilon^3 \pi c_0 \frac{\bar{v}^2 L \hat{\xi}}{t^4 \mathcal{A}} \frac{1}{\hat{\xi}^2} \frac{1}{k_1^2 k_2^2 k_3^2} \times \frac{k_1^4 \kappa_{23} + k_2^4 \kappa_{31} + k_3^4 \kappa_{12}}{(\kappa_{23} \kappa_{31} + \kappa_{12} \kappa_{31} + \kappa_{12} \kappa_{23})^{3/2}}. \quad (\text{A21})$$

-
- [1] M. B. Hindmarsh and T. W. B. Kibble, Rept. Prog. Phys. **58**, 477 (1995), hep-ph/9411342.
- [2] A. Vilenkin and E. P. S. Shellard, *Cosmic Strings and Other Topological Defects* (Cambridge University Press, Cambridge, 1994).
- [3] M. Sakellariadou, Lect. Notes Phys. **718**, 247 (2007), hep-th/0602276.
- [4] T. W. B. Kibble, J. Phys. **A9**, 1387 (1976).
- [5] A. Dabholkar, G. W. Gibbons, J. A. Harvey, and F. Ruiz Ruiz, Nucl. Phys. **B340**, 33 (1990).
- [6] E. J. Copeland, R. C. Myers, and J. Polchinski, JHEP **06**, 013 (2004), hep-th/0312067.
- [7] J. Yokoyama, Phys. Rev. Lett. **63**, 712 (1989).
- [8] L. Kofman, A. D. Linde, and A. A. Starobinsky, Phys. Rev. Lett. **73**, 3195 (1994), hep-th/9405187.
- [9] E. J. Copeland, A. R. Liddle, D. H. Lyth, E. D. Stewart, and D. Wands, Phys. Rev. **D49**, 6410 (1994), astro-ph/9401011.
- [10] S. Sarangi and S. H. H. Tye, Phys. Lett. **B536**, 185 (2002), hep-th/0204074.
- [11] G. Dvali and A. Vilenkin, JCAP **0403**, 010 (2004), hep-th/0312007.
- [12] R. A. Battye, B. Garbrecht, and A. Moss, JCAP **0609**, 007 (2006), astro-ph/0607339.
- [13] N. Bevis, M. Hindmarsh, M. Kunz, and J. Urrestilla (2007), astro-ph/0702223.
- [14] A. Gangui, L. Pogosian, and S. Winitzki, Phys. Rev. **D64**, 043001 (2001), astro-ph/0101453.
- [15] N. Bevis, M. Hindmarsh, M. Kunz, and J. Urrestilla, Phys. Rev. **D76**, 043005 (2007), arXiv:0704.3800 [astro-ph].
- [16] L. Pogosian and M. Wyman (2007), arXiv:0711.0747 [astro-ph].
- [17] J. R. Gott III, Astrophys. J. **288**, 422 (1985).
- [18] N. Kaiser and A. Stebbins, Nature (London) **310**, 391 (1984).
- [19] M. Hindmarsh, S. Stuckey, and N. Bevis (2008), 0812.1929.
- [20] C. J. A. P. Martins and E. P. S. Shellard, Phys. Rev. D **73**, 043515 (2006), arXiv:astro-ph/0511792.
- [21] A. A. Fraisse, C. Ringeval, D. N. Spergel, and F. R. Bouchet, Phys. Rev. **D78**, 043535 (2008), 0708.1162.
- [22] M. Hindmarsh, Astrophys. J. **431**, 534 (1994), astro-ph/9307040.
- [23] D. N. Spergel and D. M. Goldberg, Phys. Rev. **D59**, 103001 (1999), astro-ph/9811252.
- [24] A. Gangui and J. Martin, Phys. Rev. **D62**, 103004 (2000), astro-ph/0001361.
- [25] M. White, J. Carlstrom, M. Dragovan, and W. Holzapfel, Astrophys. J. **514**, 12 (1999), arXiv:astro-ph/9712195.
- [26] M. LoVerde and N. Afshordi, Phys. Rev. **D78**, 123506 (2008), 0809.5112.
- [27] N. Kaiser and A. Stebbins, Nature **310**, 391 (1984).
- [28] F. R. Bouchet, D. P. Bennett, and A. Stebbins, Nature **335**, 410 (1988).
- [29] N. Bevis, M. Hindmarsh, M. Kunz, and J. Urrestilla, Phys. Rev. **D75**, 065015 (2007), astro-ph/0605018.
- [30] E. Komatsu and D. N. Spergel, Phys. Rev. **D63**, 063002 (2001), astro-ph/0005036.
- [31] E. Komatsu et al. (WMAP), Astrophys. J. Suppl. **180**, 330 (2009), 0803.0547.
- [32] N. Bevis, M. Hindmarsh, M. Kunz, and J. Urrestilla, Phys. Rev. D **75**, 065015 (2007), arXiv:astro-ph/0605018.
- [33] D. P. Bennett and F. R. Bouchet, Phys. Rev. D **41**, 2408 (1990).
- [34] C. Ringeval, M. Sakellariadou, and F. R. Bouchet, J. Cosmol. Astropart. Phys. **02**, 023 (2007), arXiv:astro-ph/0511646.
- [35] T. Vachaspati and A. Vilenkin, Phys. Rev. D **30**, 2036 (1984).
- [36] D. N. Spergel et al., Astrophys. J. Suppl. Ser. **170**, 377 (2007), arXiv:astro-ph/0603449.
- [37] N. Aghanim, M. Kunz, P. G. Castro, and O. Forni, Astron. Astrophys. **406**, 797 (2003), astro-ph/0301220.
- [38] C. R. Contaldi and J. Magueijo, Phys. Rev. **D63**, 103512 (2001), astro-ph/0101512.
- [39] G. Rocha, M. P. Hobson, S. Smith, P. Ferreira, and A. Challinor, Mon. Not. R. Astron. Soc. **357**, 1 (2005), arXiv:astro-ph/0406136.
- [40] N. Bartolo, E. Komatsu, S. Matarrese, and A. Riotto, Phys. Rept. **402**, 103 (2004), astro-ph/0406398.
- [41] J. Ruhl et al., in *Millimeter and Submillimeter Detectors for Astronomy II*, edited by J. Zmuidzinas, W. S. Hol-

- land, and S. Withington (2004), vol. 5498 of *Proceedings of the SPIE*, p. 11, arXiv:astro-ph/0411122.
- [42] K. M. Huffenberger and U. Seljak, *New Astron. Rev.* **10**, 491 (2005), arXiv:astro-ph/0408066.
- [43] R. Barker *et al.* (AMI Collaboration), *Mon. Not. R. Astron. Soc.* **369**, L1 (2006), arXiv:astro-ph/0509215.